数理解析研究所講究録
635 巻 1987 年 234-255

Bifurcation Analysis of A Cusp-Constrained Piecewise Linear Circuit

徳永隆治
Ryuji Tokunaga
Department of Electrical Engineering,
Waseda Unversity, Tokyo, 160, Japan.

ABSTRACT

This paper performs a detailed bifurcation analysis of a cusp-constrained circuit in terms of the quantity "*rotation-jump ratio*". This turns out to be a very natural quantity to analyse various interesting bifurcation phenomena observed in the circuit.

I. INTRODUCTION

This paper performs a detailed bifurcation analysis of a *constrained* "Lorenz"-like attractor observed from an extremely simple piecewise-linear circuit , in terms of the "*rotation-jump ratio*". Many interesting bifurcation structures are descernible.

One of the motivations of this paper came from recent works on *constrained attractors*. Oka and Kokubu [1] observed a "Lorenz"-like attractor which is constrained to a smooth cusp surface. Ushiki and Lozi [2] analysed bifurcations of "confiner" and "anti-confiner" of a constrained "Lorenz"-like attractor. Apparently, the reason for studying constrained attractors is its ease of performing bifurcation analysis. For example, no global two-parameter bifurcation analysis of the *original* Lorenz equation has been done mainly because of its complexity.

Our bifurcation analysis proceeds in the following steps:

(1) Experimantal observations.
(2) Confirmation by computer simulations.
(3) Analysis of typical trajectories in terms of the piecewise-linear geometry of the dynamics.
(4) Derivation of the *rigorous* 1-D map.
(5) Construction of an approximate 1-D map.
(6) Detailed bifurcation analysis of the approximate 1-D map.
(7) 2-parameter bifurcation analysis.

The "rotation-jump ratio" defined below turns out to be a very natural quanitiy for analysing those bifurcations.

/

1.1 System and Attractor

We have recently reported on a "Lorenz"-like attractor from a circuict whose nonlinear element consist of two uncoupled piecewise-linear resistors [3]. This circuit is shown in Fig.1(a), where V-NIC (resp. I-NIC) denotes a voltage (resp. current) inversion negative impedance converter. All elements in this circuit are linear except for the piecewise-linear registors $g_1(\cdot)$, $g_2(\cdot)$ which are described in Fig.1(b). The dynamics of this circuit is given by

$$
\begin{aligned}
L\frac{di_L}{dt} &= v_{c_1} - R_1 i_L \\
C_1\frac{dv_{c_1}}{dt} &= g_1(v_{c_1} - v_{c_2}) - g_2(v_{c_1} + v_{c_2}) - G_2 v_{c_1} - i_L \\
C_2\frac{dv_{c_2}}{dt} &= g_1(v_{c_1} - v_{c_2}) + g_2(v_{c_1} + v_{c_2}) + G_3(v_{c_2} - E)
\end{aligned}
\tag{1.1}
$$

$$
g_1(x) = \frac{1}{2}\{(m_0 - m_1)|x| + (m_0 + m_1)x\},\quad g_2(x) = \frac{1}{2}\{(m_0 - m_1)|x| - (m_0 + m_1)x\} \tag{1.2}
$$

and vc_1,vc_2 and i_L denote the voltage across C_1, the voltage across C_2 and the current through L, respectively. Using the parameter values

$$L = 13.0,\ C_1 = 6.8,\ C_2 = 47.0,\ R_1 = 1.7,\ G_2 = 1.5,\ G_3 = 1.0,\ E = 1.0,\ m_0 = 1.48,\ m_1 = 0.56, \tag{1.3}$$

we observed a "Lorenz"-like attractor (3). In this paper, we choose a different set of parameter values; namely,

$$L = 0.4,\ C_1 = 0.001,\ C_2 = -1.0,\ R_1 = -2.0,\ G_2 = 0,\ G_3 = 2.0,\ E = -1.0,\ m_0 = -1.0,\ m_1 = 0.5. \tag{1.4}$$

A different piecewise-linear function is chosen for $g_1(\cdot)$ and $g_2(\cdot)$, as shown in Fig.1(c). The new circuit which realizes (1.4) and Fig.1(c) is shown in Figure 2, where C_1 is replaced by an open circuit, i.e., C_1 is considered as a *parastic* element. From this dynamics, we observed strange attractor whoes projections are shown in Fig.3.

Now let us consider the behavior of a typical trajectory in Fig.4. If an initial condition is picked in the centre of the righthand-side spiral, the resulting trajectory will rotate around the righthand-side centre in a counterclockwise direction while increasing amplitude. After several rotations, trajectory hits the righthand-side *fold*, then jumps to the opposite side in a rapid motion. Then it starts to rotate around the lefthand-side centre in a clockwise direction. After several rotations, it hits the lefthand-side fold and jumps to the righthand-side region again. The same process is repeated many time in a random manner.

These observations indicate that *rotations* and *jumps* are very important quantities describing the nature of trajectories. We will define, therefore,

$$\boxed{\rho = n / m,} \tag{1.5}$$

where n and m denote the number of *rotations* and the number of *jumps*, respectively. This "rotation-jump ratio" plays an important role throughout our bifurcation analysis.

Note that (1.1)~(1.3) is *not* the Lorenz equation [4] and yet it exhibits "Lorenz"-like attractor. The piecewise-linearity of the dynamics simplifies the subsequent analysis in a significant manner.

Figure 1

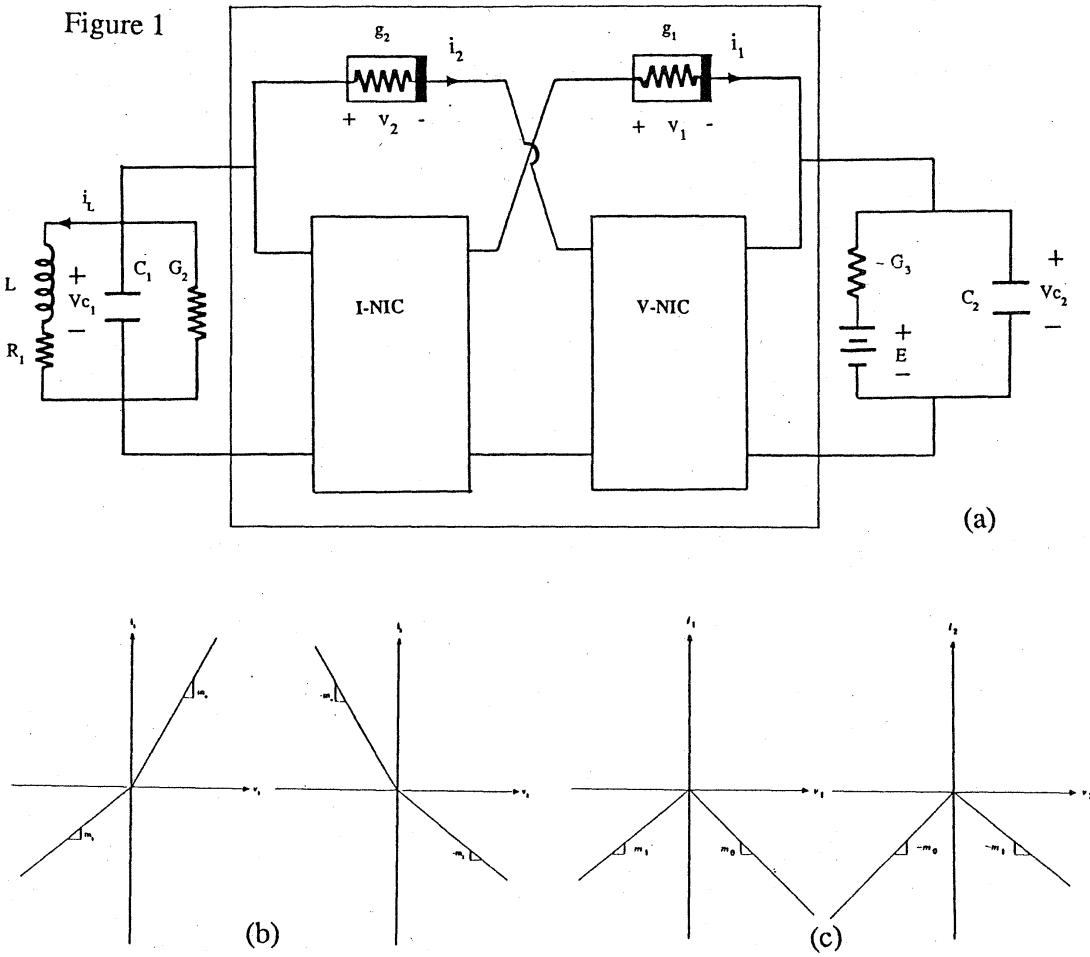

Figure 2

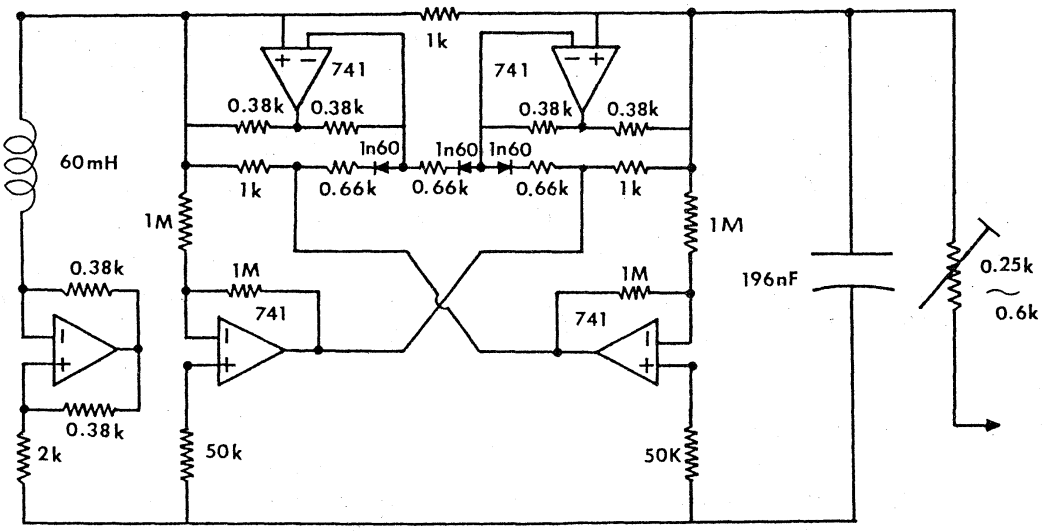

Figure 3

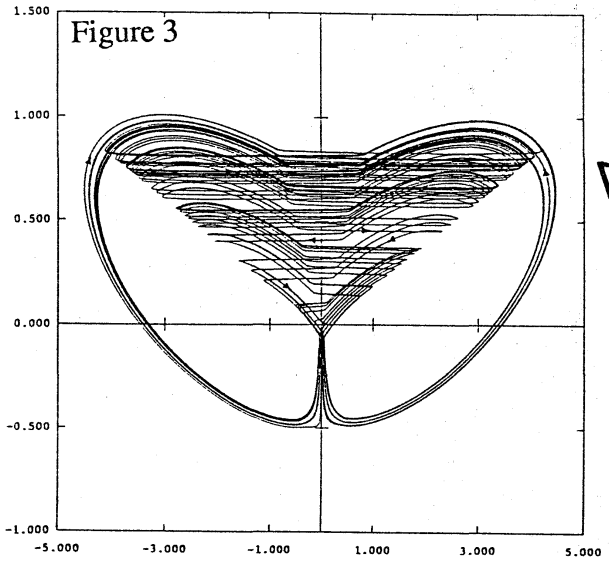

Figure 4

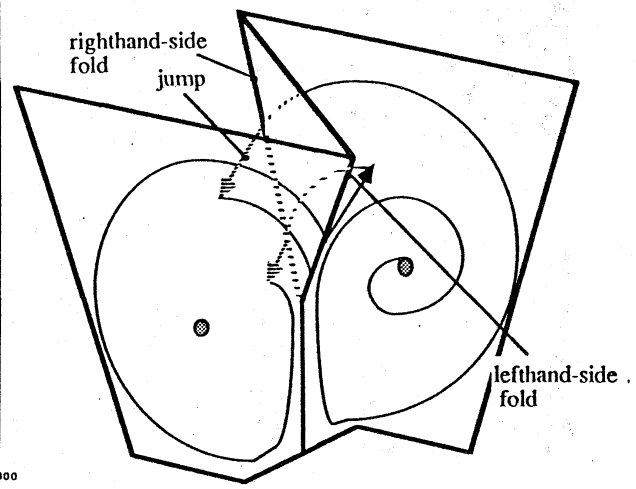

Figure 5

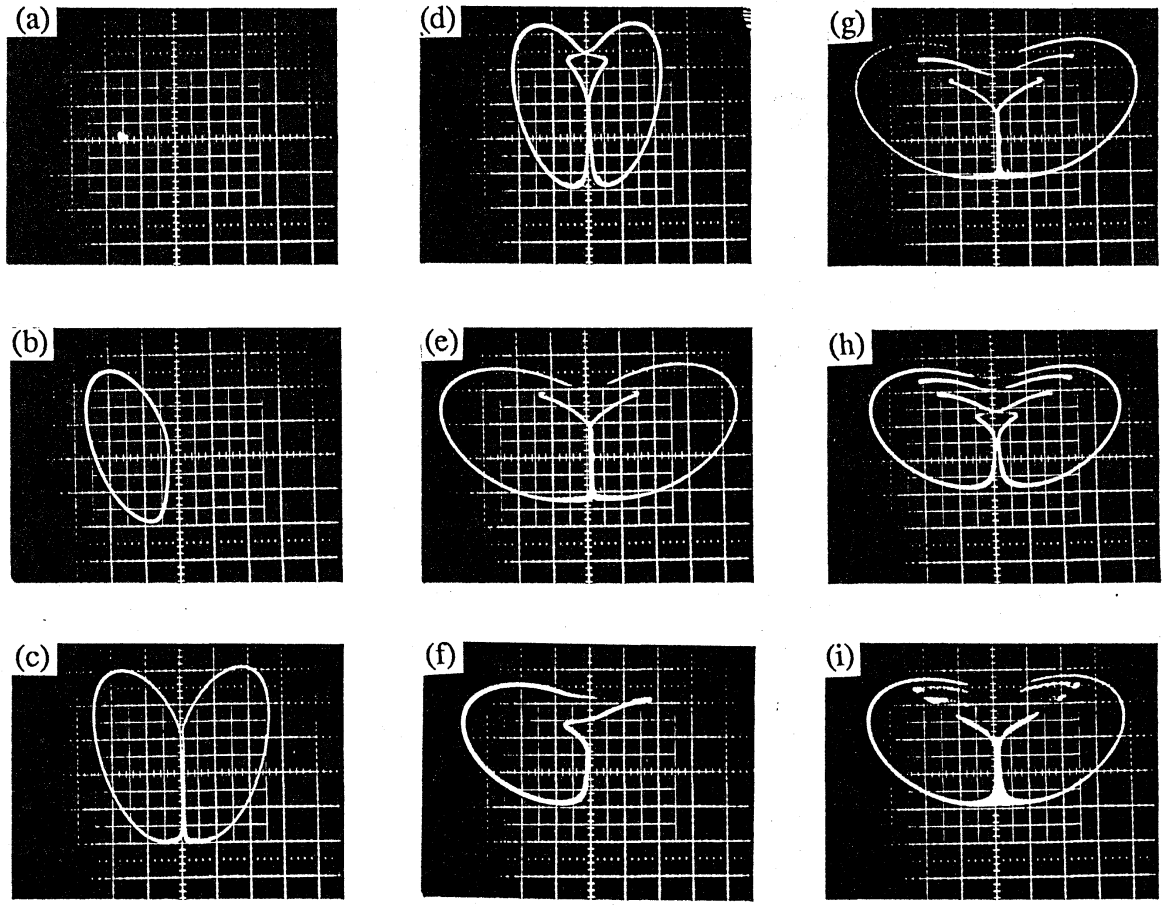

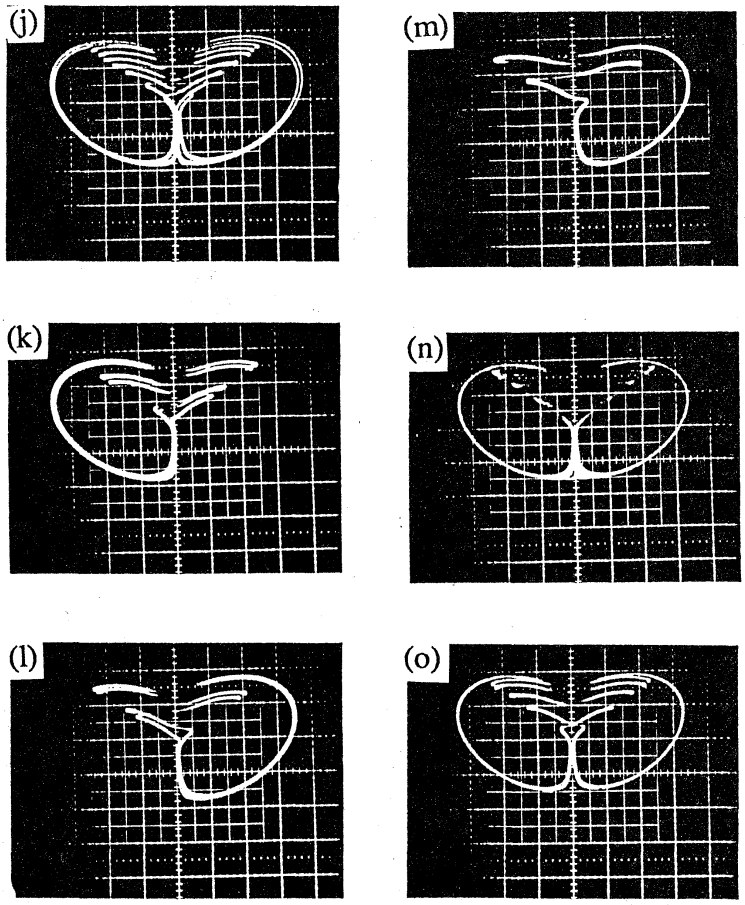

(a) Vertical scale: 0.4 V/div.
Horizontal scale: 2.0 V/div.
(b) Vertical scale: 0.4 V/div.
Horizontal scale: 2.0 V/div.
(c) Vertical scale: 0.4 V/div.
Horizontal scale: 2.0 V/div.
(d) Vertical scale: 0.4 V/div.
Horizontal scale: 2.0 V/div.
(e) Vertical scale: 0.5 V/div.
Horizontal scale: 1.0 V/div.
(f) Vertical scale: 0.5 V/div.
Horizontal scale: 1.0 V/div.
(g) Vertical scale: 0.5 V/div.
Horizontal scale: 1.0 V/div.
(h) Vertical scale: 0.5 V/div.
Horizontal scale: 1.0 V/div.
(i) Vertical scale: 0.5 V/div.
Horizontal scale: 1.0 V/div.
(j) Vertical scale: 0.5 V/div.
Horizontal scale: 1.0 V/div.
(k) Vertical scale: 0.5 V/div.
Horizontal scale: 1.0 V/div.
(l) Vertical scale: 0.5 V/div.
Horizontal scale: 1.0 V/div.
(m) Vertical scale: 0.5 V/div.
Horizontal scale: 1.0 V/div.
(n) Vertical scale: 0.5 V/div.
Horizontal scale: 1.0 V/div.
(o) Vertical scale: 0.5 V/div.
Horizontal scale: 1.0 V/div.

Figure 6

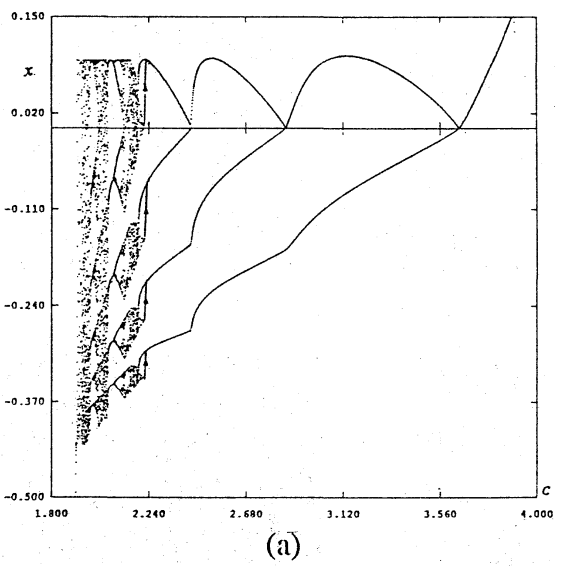

(a)

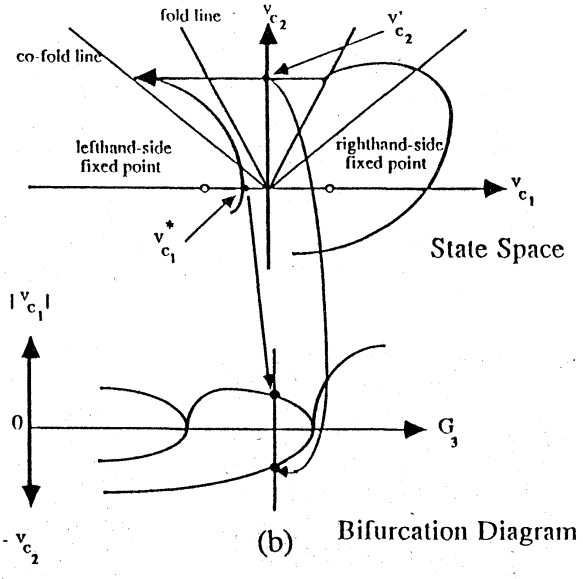

1.2 Experimental Observation of the G_3-Bifurcations

Consider first the bifurcations resulting from varying the conductance G_3. At G_3= 4.0, a pair o non-symmetric periodic orbits are born via Hopf bifurcation. As G_3 decreases, the amplitude of each orbit gets larger until they merge with each other, forming a symmetric periodic orbit, via a reverse symmetry-breaking bifurcation at $G_3 \cong$ 3.646, (see Fig.5(a)~(d)). In the same manner, as G_3 decreases, the amplitudes of the right and the left cycle grow larger, until they become tangent to itself and split into a pair of non-symmetric periodic orbits via symmetry breaking-bifurcation at $G_3 \cong$ 2.86, (see Fig.5(e)~(f)). The same process occurs once again, with the periodic orbits merging with each other into a symmetric periodic orbit at $G_3 \cong$ 2.433, (see Fig.5(g)~(h)). This symmetric periodic orbit, however, soon disappears and a chaotic state suddenly appears at $G_3 \cong$ 2.220. Subsequently, several small periodic windows with high period appear via reverse period doubling and then disappear via an inttermittency process. Then follows a periodic window at $G_3 \cong$ 2.17 via reverse doubling, (see Fig.5(i)~(m)). At $G_3 \cong$ 2.11, this periodic orbit suddenly breaks into a chaotic state via intermittency. Then, several small periodic windows appear and disappear in quick succession before a large periodic window appear at $G_3 \cong$ 1.995. Then chaos appears once again via intermittency, disappears abruptly at $G_3 \cong$ 1.94, (Fig.5(n)~(o)).

Figure 6(a) shows the bifurcation diagram of the above bifurcation sequence, where the horizontal axis denotes G_3 and the vertical axis denotes the state.
This diagram is constructed in following manner:

Consider Fig.6(b) where a part of a typical trajectory is drawn together with fixed points and related sets on the (v_{C1},v_{C2})-plane. The fold (resp. co-fold) line is the set of points where a trajectory "takes off" (resp."lands") for a jump. (see section II for details.) If an orbit hits the v_{C2}= 0 -plane downwards for instance at $(i_L^*,v_{C1}^*,0)$, then $|v_{C1}^*|$ is plotted versus G_3. And if the orbit hits the v_{C1}= 0 -plane for instance at $(i_L',0,v_{C2}')$, then v_{C2}' is plotted versus G_3 (see Fig.6(b)).

This bifurcation sequence can be roughly sumarized by the following schematic representation:

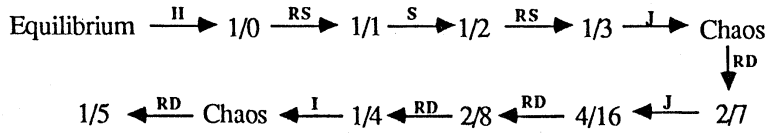

where"**H**","**RD**","**S**","**RS**","**I**", and "**J**" denote the Hopf bifurcation, reverse period doubling, symmetry breaking bifurcation, reverse symmetry breaking bifurcation, intermittency and jump, and the fractional numbers denote the associated ρ. If a trjectory is non-periodic we simply let ρ be undefined. It is very interesting to observe that the sequence of ρ described above can be characterized by a period-adding sequence of the circle map [5] even though (1.5) is *not* the rotation number. In section II, a detailed study is made of the trajectories in terms of piecewise-linear geometry.

In section III, a one-dimensional map is constructed and used to analyse the one-parameter bifurcation phanomena. In section IV, we describe the two-parameter bifurcations and fractalization phenomena in two-dimensional parameter space.

II. Constrained System

If we define

$$a = R_1 m_0,\ b = \frac{-G_2}{m_0},\ c = \frac{G_3}{m_0},\ \tau = \frac{m_0 t}{C_2},\ x = \frac{i_L}{G_3 E},\ y = \frac{m_0 v_{C_1}}{G_3 E},\ z = \frac{m_0 v_{C_2}}{G_3 E},$$
$$\alpha = \frac{-C_2}{C_1},\ \varepsilon = \frac{-C_1}{C_2},\ m = \frac{-m_1}{m_0}, \tag{2.1}$$

we can rescale (1.1) and transform it into the following dimensioless form:

$$\frac{dx}{d\tau} = \alpha(-y + ax)$$
$$\varepsilon \frac{dy}{d\tau} = f_1(y - z) - f_2(y + z) + by + x \tag{2.2}$$
$$\frac{dz}{d\tau} = -f_1(y - z) - f_2(y + z) - cz - 1$$

where

$$f_1(x) = \frac{1}{2}\{-(m+1)|x| + (m-1)x\},\quad f_2(x) = \frac{1}{2}\{-(m+1)|x| - (m-1)x\} \tag{2.3}$$

Define the subsets

$$D_1 = \{(x,y,z) \mid -z \le y \le z\},\ D_0 = \{(x,y,z) \mid z \le y \le -z\}$$

$$D_+ = \{(x,y,z) \mid -y \le z \le y\},\ D_- = \{(x,y,z) \mid y \le z \le -y\}.$$

As ε approaches zero, the state of this system is constrained to lie in a surface Σ defined by :

$$\Sigma = \{(x,y,z) \mid f_1(y-z) - f_2(y+z) + by + x = 0\}.$$

In each of D_0, D_1 and $D_\pm$, the set Σ are given by

$$\Sigma_1 = \{(x,y,z) \mid x + (b-2)y = 0\},\qquad \Sigma_0 = \{(x,y,z) \mid x + (b+2m)y = 0\},$$

$$\Sigma_\pm = \{(x,y,z) \mid x + (b-1+m)y \pm (m+1)z = 0\}.$$

If

$$\frac{\partial}{\partial y}\left[\frac{dy}{d\tau}\right]_{x \in D_0} = b-2 < 0,\ \frac{\partial}{\partial y}\left[\frac{dy}{d\tau}\right]_{x \in D_1} = b+2m > 0,\ \frac{\partial}{\partial y}\left[\frac{dy}{d\tau}\right]_{x \in D_\pm} = m-1+b < 0,$$

hold, then Σ_0 and $\Sigma_\pm$ are *stable* constrained surfaces, while Σ_1 is an*unstable* constrained surface. Under this condition the surface:

$$\Sigma_0 = \Sigma^s{}_0 \cup \Sigma^u{}_1 \cup \Sigma^s{}_+ \cup \Sigma^s{}_-,\qquad O = \Sigma^s{}_0 \cap \Sigma^u{}_1 \cap \Sigma^s{}_+ \cap \Sigma^s{}_-,$$

represent a *pieacewise-linear cusp surface* and cusp point respectively where the super script "s" (resp. "u") denotes "stable" (resp. "unstable"). Define the following important subsets by

---

† $\rho = 1/0$ means that an orbit is characterized by 1 rotation with no jump.

$U_+ = \{(x,y,z)|\ y = z\}$, $U_- = \{(x,y,z)|\ y = -z\}$,
$F_\pm = U_\pm \cap \Sigma^s_\pm = \Sigma^u{}_1 \cap \Sigma^s_\pm$, $F^c{}_+ = S_- \cap \Sigma^s_+$,
$F^c{}_- = S_+ \cap \Sigma^s_-$, $F_\pm = \{(x,y,z)|\ z=0\} \cup \Sigma^s_\pm$,

where $S_\pm$ denotes a plane containing $F_\pm$ and is normal to the xz-plane, $U_\pm$ denotes the boundaries between the linear subsets, $F_\pm$ denotes the *fold* lines of $\Sigma^s_\pm$, i.e., the "cliff" of the surface, $F^c{}_\pm$ denotes the *co-fold* lines of $\Sigma^S_\pm$, i.e., the "shadow" of the fold line on the opposite stable surface, (see Fig.7). Except for D_1, there are three fixed points in each linear region; namely,

$P_\pm = (\pm k, \pm ak, (ab + a - am - 1)k) \in \Sigma^s_\pm$. $P_0 = (0,0,-1/(2+c)) \in \Sigma^s{}_0$

where $k^{-1} = a(m+1)^2 - [a(b+1-m)-1](c+1-m)$. Assuming $ab + a - am - 1 = 0$ and $b = 0$, then, $P_\pm$ can be rewritten by $P_\pm = (\pm 1/(2a-1), \pm a/(2a-1), 0) \in \Sigma^s_\pm$. Figure 7 shows the relative position between boundaries and these subsets.

Consider the projection of the slow vector field on Σ^s_i onto the (y,z)-plane i=0,1,±. From (2.2) and (2.3), we obtain the following second order differencial equations:

$$\begin{array}{ll} \xi_0 : x \in \Sigma^s_0 & \xi_\pm : x \in \Sigma^s_\pm \\ \frac{dy}{d\tau} = \alpha \frac{(2a-1)}{2} y & \frac{dy}{d\tau} = \frac{(2a-1)^2}{a} y \pm \frac{(1-2a)(1+ac+\alpha a^2)}{a} z \pm (1-2a) \\ \frac{dz}{d\tau} = -(2+c)z - 1 & \frac{dz}{d\tau} = \pm \frac{2a-1}{a} y - \frac{1+ac}{a} z - 1 \end{array} \qquad (2.4)$$

where $x = (y,z)$.
In the same way, the projection of the subsets are given by

$\Sigma^s{}_{0+} = \{(y,z)|\ z \le 0, y \ge 0, z \le -y\}$, $\Sigma^s{}_{0-} = \{(y,z)|\ z \le 0, y \le 0, z \le y\}$
$\Sigma^s{}_0 = \Sigma^s{}_{0+} \cup \Sigma^s{}_{0-}$, $\Sigma^s{}_+ = \{(y,z)|\ -y \le z \le y\}$
$\Sigma^s{}_- = \{(y,z)|\ y \le z \le -y\}$
$F_\pm = \{(x,y,z)|\ z = \pm y, \pm y \ge 0\}$, $F^c{}_\pm = \{(x,y,z)|\ y = \pm(4a-3)z, \pm y \ge 0\}$
$H_\pm = \{(x,y,z)|\ z = 0, \pm y \ge 0\}$, $L_\pm = \{(x,y,z)|\ -z = \pm y, \pm y \ge 0\}$
$p_\pm = (\pm a/(2a-1), 0)$, $p_0 = (0, -1/(a+c))$.

The eigenvalues of p_0 are given by $\alpha_0 = \alpha(a - 1/2)$, $\beta_0 = -(2+c)$.
If $a > 1/2$ holds, then

$E^u{}_+(p_0) = \{(y,z)|\ z = -1/(2+c), 0 \le y \le 1/(2+c)\}$
$E^u{}_-(p_0) = \{(y,z)|\ z = -1/(2+c), -1/(2+c) \le y \le 0\}$
$E^s(p_0) = \{(y,z)|\ y = 0, z \le 0\}$

where $E^u{}_\pm(p_0)$ (resp. $E^s(p_0)$) denotes the unstable eigenspace (resp. stable eigenspace) corresponding to α (resp. β).

Note that p_0 is a saddle type fixed point. On the other hand, the eigenvalues of $p_\pm$ are given by the solution of the following characteristic equation: $\lambda^2 - (4a - 4 - c)\lambda + \alpha(2a - 1)^2 = 0$. If $(4a - 4 - c)^2 - 4\alpha(2a - 1)^2 < 0$ holds, then $p_\pm$ is a focus. Its eigen values consists of a complex conjugate pair: $\sigma \pm j\omega = (2a - 2 - c/2) \pm j(-(2a - 2 - c/2)^2 + \alpha(2a - 1)^2)^{1/2}$.

If $\sigma = (2a - 2 - c/2) > 0$ holds, thus $p_\pm$ is an unstable forcus. Therefore $c = 4(a - 1)$ is the condition for the onset of Hopf bifurcation. Let $\psi^\tau_\pm(x)$ be the trajectory of $\xi_\pm$ which starts from an initial condition, $x \in \Sigma^s_\pm$ and let $J_\pm$ be the map: $F_\pm \to F^c_\pm$ which corresponds to the jump defined by

$$J_\pm(z_\pm) = (\pm\frac{z}{3-4a}, z), \quad \text{where } z_\pm = (\pm z, z) \in F_\pm.$$

Define the following important points which determine the fate of the trajectories:

$A_\pm$ = a point where the trajectory of $\xi_\pm$ is tangent to $L_\pm$,
$B_\pm$ = a point where the trajectory of $\xi_\pm$ is tangent to $F^c_\pm$,
$C_\pm = L_\pm \cap E^u_\pm(p_0)$, $\quad o = (0,0)$,
$a_\pm$ = the first point where $\psi^\tau_\pm(A_\pm)$ hits $H_\pm$ with $\tau < 0$,
$b_\pm$ = the first point where $\psi^\tau_\pm(B_\pm)$ hits $H_\pm$ with $\tau > 0$,
$c_\pm$ = the first point where $\psi^\tau_\pm(C_\pm)$ hits $H_\pm$ with $\tau > 0$,
$d_\pm$ = the first point where $\psi^\tau_\pm(o)$ hits $H_\pm$ with $\tau < 0$,
$e_\pm = J^{-1}_\pm(od_\pm \cap F^c_\pm)$
$g_\pm$ = the first point where $\psi^\tau_\pm(C_\pm)$ hits $F_\pm$ with $\tau > 0$,

where $od_\pm$ denotes a segment of trajectory between o and $d_\pm$, (see Fig.8).

III Analysis of the Bifurcation Phenomena

3.1 Rigorous one-dimensional map P

One of the greatest advantages of the piecewise-linearity of our circuit is the fact that we can derive an *exact* 1-D map.

In order to derive the exact 1-D map P, We first identify $\Sigma^s_+ \cup \Sigma^s_{0+}$ and $\Sigma^s_- \cup \Sigma^s_{0-}$, and consider only the righthand-side. Therefore the subscripts "+" and "-" of all symbols are neglected. The map J: $F \to F^c$ is defined by

$$J(z) = (\frac{z}{4a-3}, z) \qquad \text{where } z = (z, z) \in F.$$

Figure 7

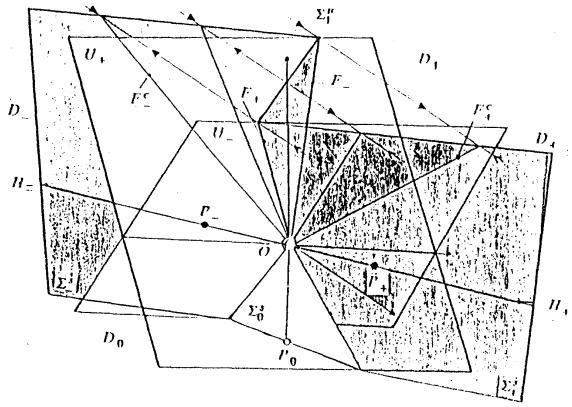

Figure 8

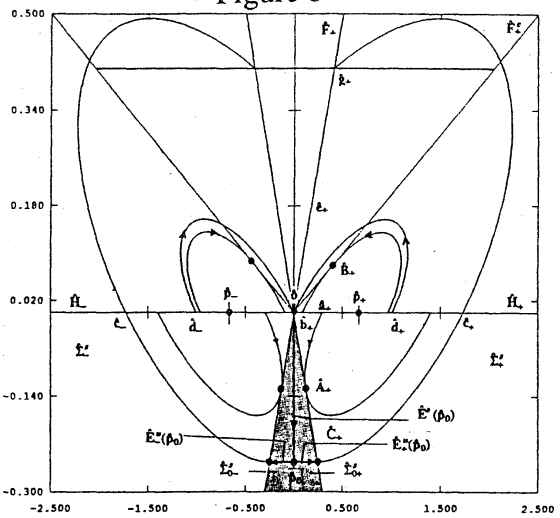

Figure 9

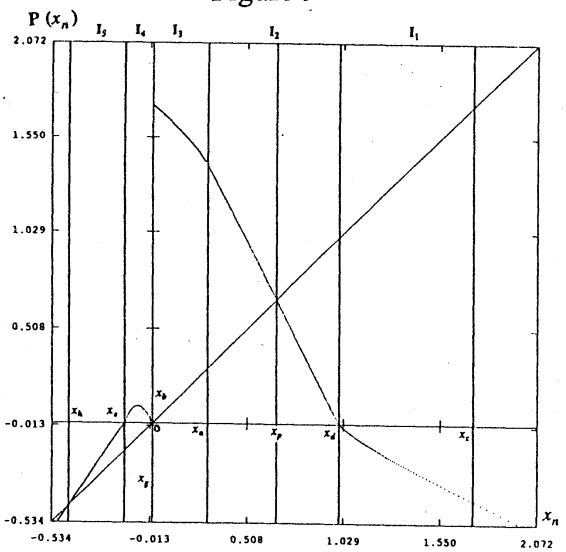

Figure 10

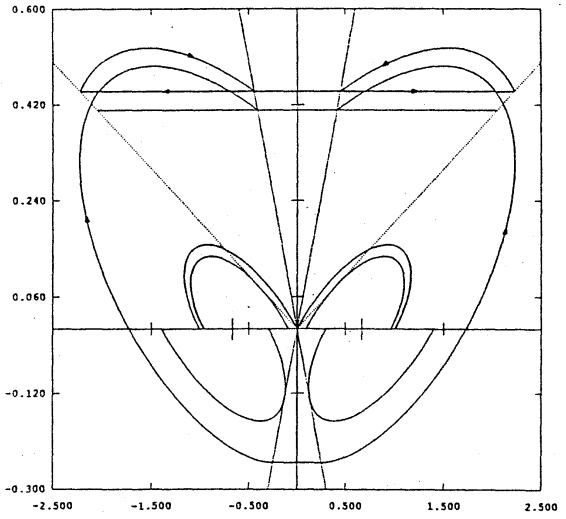

Figure 11

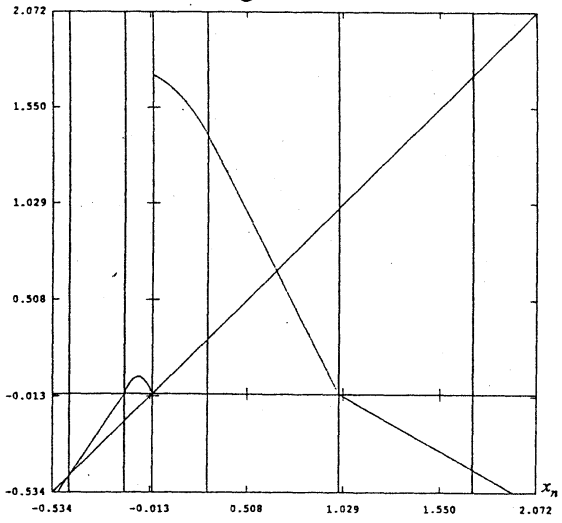

Figure 12

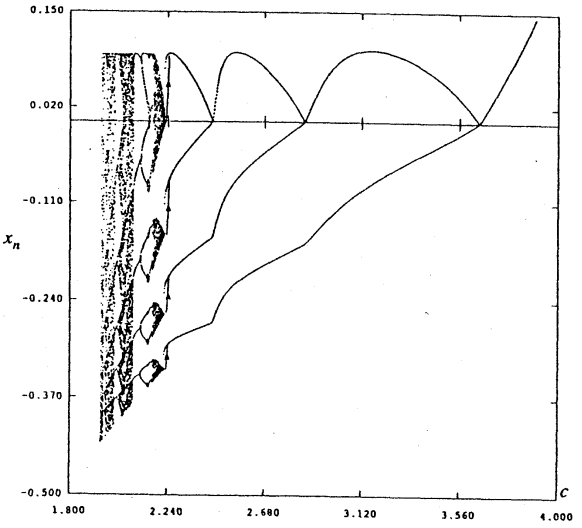

Define the map $\Phi : F \cup H \to \mathbb{R}$ by

$$\Phi \cdot x = \begin{cases} \langle e_0, x \rangle & \text{if } x \in H \\ -\langle e_0, x \rangle & \text{if } x \in F \end{cases}$$

where $e_0 = (1,0)$ and $\langle , \rangle$ denotes the inner product. Points which belong to F and H are mapped by Φ into the following points:

$$x_a = \Phi \cdot a\,,\ x_b = \Phi \cdot b,\ x_c = \Phi \cdot c\,,\ x_d = \Phi \cdot d\,,\ x_e = \Phi \cdot e\,,\ x_g = \Phi \cdot g\,,\ x_p = \Phi \cdot p\,.$$

Consider the following subsets:

$$I_1 = [x_d, \infty),\ I_2 = [x_a, x_d],\ I_3 = [0, x_a],\ I_4 = [x_e, 0],\ I_5 = (-\infty, x_e],$$

and define the one dimensional map by

$$P : \mathbb{R} \to \mathbb{R} \begin{cases} P_1 & \text{if } x \in I_1 \\ P_2 & \text{if } x \in I_2 \\ P_3 & \text{if } x \in I_3 \\ P_4 & \text{if } x \in I_4 \\ P_5 & \text{if } x \in I_5 \end{cases}$$

where P_i, $(i = 1,2,3,4,5)$ are calculated as follow:

Since ξ_0 and ξ (recall (2.4)) are linear differential equations, one can solve for the solution in each linear region. Using these solutions, the map P_i $(i = 1,2,3,4,5)$ are given *exactly* by

$$P_1(x) : I_1 \to I_4 \cup I_5 \tag{3.1}$$

$$P_1(x) = \frac{x_p k_3 \sin\theta_1}{\cos\theta_1 + (k - k_3 - k_4)\sin\theta_1} \quad \text{where } x = \frac{-x_p e^{-k\theta_1}}{\cos\theta_1 + (k - k_3 - k_4)\sin\theta_1} + x_p,\ \ \text{atan}\left(\frac{1}{k_4 + k_3 - k}\right) < \theta_1 \le \pi$$

$$P_2(x) : I_2 \to I_1 \cup I_2 \cup I_3 \tag{3.2}$$

$$P_2(x) = -e^{k\pi}(x - x_p) + x_p$$

$$P_3(x) : I_3 \to I_1 \cup I_2 \tag{3.3}$$

$$P_2(x) = \frac{x_{p_0} e^{k\theta_3^p}(\cos\theta_3^p + (k - k_2 - k_4)\sin\theta_3^p)\, e^{\alpha_0 t_3}(1 - e^{\beta_0 t_3})}{e^{\alpha_0 t_3} - e^{\beta_0 t_3}} - x_p e^{k\theta_3^p}(\cos\theta_3^p + (k - k_4)\sin\theta_3^p) + x_p$$

where $u_x = \dfrac{x_{p_0}(1 - e^{\beta_0 t_3})}{e^{\alpha_0 t_3} - e^{\beta_0 t_3}}$, $u_p = \dfrac{x_{p_0} e^{\alpha_0 t_3}(1 - e^{\beta_0 t_3})}{e^{\alpha_0 t_3} - e^{\beta_0 t_3}}$, $x = \dfrac{-x_p e^{-k\theta_3^x}}{\cos\theta_3^x + (k - k_3 - k_4)\sin\theta_3^x} + x_p$

$$\theta_3^x = \text{atan}\left(\frac{u_x}{x_p k_3 - u_x(k + k_3 - k_4)}\right), \qquad \theta_3^p = \text{atan}\left(\frac{u_p}{(k_1 + k_3 - k)u_p - x_p k_3}\right), \quad 0 < t_3 < \infty,$$

$$P_4(x) : I_4 \to I_1 \cup I_2 \cup I_3 \qquad (3.4)$$

$$P_4(x) = e^{k\theta_4}[\cos\theta_4 + (k-k_4)\sin\theta_4](-nx - x_p) - k_2 x e^{k\theta_4}\sin\theta_4 + x_p$$

where $\theta_4 = \text{atan}\left(\frac{x}{k_3(-nx - x_p) - x(k-k_1)}\right)$

$$P_5(x) : I_5 \to I_4 \cup I_5 \qquad (3.5)$$

$$P_5(x) = -e^{k\theta_5}[\{\cos\theta_5 + (k-k_4)\sin\theta_5\}(-nx - x_p) - k_2 x\sin\theta_5] - x_p$$

where

$$x = \frac{-x_p(\cos\theta_5 + (k-k_3-k_2)\sin\theta_5 - e^{-k\theta_5}}{(n-1)\cos\theta_5 + ((k-k_3-k_4)n + k_1+k_2-k)\sin\theta_5}, \quad \text{atan}\left(\frac{x_e}{(-nx_e - x_p)k_3 - (k-k_1)x_e}\right) \le \theta_5 < \text{atan}\left(\frac{1-n}{n(k-k_3-k_4)+k_1+k_2-k}\right)$$

where $k = \sigma/\omega$, $k_1 = (2a-1)^2/\omega a$, $k_2 = (1-2a)(1+ac+\alpha a^2)/\omega a$, $k_3 = (2a-1)/\omega a$, $k_4 = -(1+ac)/\omega a$, $x_{p0} = 1/(2+c)$ $n = 4a-3$, and $\text{atan}(x) = 0.5\,\pi\,(1-\text{sgn}(x)) + \tan^{-1}(x)$. Note that P_1 P_3 P_5 are described implicitly, while P_2 and P_4 are described explicitly.

Figure 9 shows the x-P(x) graph for c = 2.0. Let us describe the relationship between the 1-D map **P** and the constrained system. Map **P** is discontinuous at x=0. This means that (0,0) corresponds to the cusp-point ***o***, while $(0,x_c)$ corresponds to ***c***.

Note that there is another unstable fixed point, say (x_h, x_h), which belongs to I_5. It corresponds to a 0/1-periodic orbit. Since it is unstable, it can not be observed by experiment or Runge-Kutta. Figure 10 shows the confirmation of this unstable periodic orbit. Recall that when the attractor disappears, there is a periodic orbit. This situation corresponds to a collision between the attractor and the unstable periodic orbit, i.e.,"boundary crisis". For this map, the condition for boundary crisis is given by $x_h = P(x_c) = x_g$. This map has two extrema. One of them belongs to the interval I_4, say (x_f, x_b), and the other is $(0,x_c)$.

The derivative at $(0,x_c)$ is given by

$$\frac{dP(x)}{dx} = \frac{dP(x)}{d\theta_3^p}\frac{d\theta_3^p}{du_p}\frac{du_p}{dt_3}\frac{dt_3}{du_x}\frac{du_x}{d\theta_3^x}\frac{d\theta_3^x}{dx}$$

Note that the following relations hold.

$$1 \le \left|\frac{dP(x)}{du_p}\right| < e^{k\pi}, \quad 1 \le \left|\frac{du_x}{dx}\right| < e^{k\pi}, \quad \lim_{x\to+0}\left|\frac{du_p}{du_x}\right| = \begin{cases} 0 & \text{if } k' > 1 \\ \infty & \text{if } k' < 1 \end{cases}$$

where $k' = \left|\frac{\beta_0}{\alpha_0}\right|$.

Hence

$$\lim_{x\to+0}\left|\frac{dP(x)}{du_x}\right| = \begin{cases} 0 & \text{if } k' > 1 \\ \infty & \text{if } k' < 1 . \end{cases} \qquad (3.6)$$

This is a very important property which strongly affects the stability of periodic orbits. The condition for the existence of an extremum is given by $\alpha < (4+2c)/(2a-1)$. Note that this condition holds everywhere in the above bifurcation sequence.

3.2 Approximate One-dimensional Map P'

The 1-D map P_i obtained above is still too time consuming to deal with directly. We will, therefore, construct an approximate 1-D map P'_i in the following explicit function:

$$P'_1(x) = A_1(x-x_d), \quad P'_{2r}(x) = A_2(x-x_p)+x_p, \quad P'_{2l}(x) = A_2(x-x_p)+x_p,$$
$$P'_3(x) = A_3 e^{2x} x^k + x_c, \quad P'_4(x) = A_4 x\,(x-x_e), \quad P'_5(x) = A_5(x-x_e),$$

where $A_1 = x_g/(x_c-x_d)$, $A_2 = -e^{k\pi}$, $A_3 = (x_l-x_c)/(x_a^k - e^{2x_a})$, $A_4 = -4x_b/x_e$, $A_5 = x_h/(x_h-x_e)$, and $x_l = P(x_a)$. We choose the function P'_3 which satisfies the condition (3.6). Note that P'_{2r} and P'_{2l} are exactly the same as P_2. By Newton-Raphson iteration, one can calculate x_a, x_b, x_c, x_d, x_e, x_f, x_g, x_h, x_l and x_p, from (3.1)~(3.5), and determine the five parameters A_i (i=1,2,3,4,5).

Figure 11 shows the approximation of P, and Figure 12 shows the bifurcation diagram, (compare with Fig.9 and Fig.6 respectively). Observe that the bifurcation phenomena of this map is qualitatively the same as the original syatem. We assert therefore that one can examine the bifurcation phenomena of the original system by using this approximate map.

Let us define next the following:

$$I'_1 = [x_d, x_c], \quad I'_{2r} = [x_p, x_d], \quad I'_{2l} = [x_a, x_p], \quad I'_3 = [0, x_a], \quad I'_4 = [x_e, 0], \quad I'_5 = [x_h, x_e],$$
$$I'_r = I'_{2l} \cup I'_3, \quad I'_l = I'_4 \cup I'_5, \quad I' = I'_r \cup I'_1,$$

$$P'_r = \begin{cases} P'_1 & \text{if } x \in I'_1 \\ P'_{2r} & \text{if } x \in I'_{2r} \end{cases}, \qquad P'_l = \begin{cases} P'_{2l} & \text{if } x \in I'_{2l} \\ P'_3 & \text{if } x \in I'_3 \end{cases}$$

Note that $P'_r : I'_r \to I'_{2r} \cup I'_1$ is a homeomorphism. Hence, the approximate map is defined by

$$P'(x) : I' \to I' = \begin{cases} P'_r(P'_l(x)) & \text{if } x \in I'_r \\ P'_4(x) & \text{if } x \in I'_4 \\ P'_5(x) & \text{if } x \in I'_5 \end{cases}$$

Figure **13** shows the schematic illustration of P'(x) and its orbit.

3.3 Analysis of One-Parameter Bifurcation Phenomena

We are now ready to analyse the bifurcation phenomena. Let us first see how the "rotation-jump ratio" defined for the original dynamics (see(1.5)) naturally carries over to the 1-D map P'. Consider the following orbit generated by P' (see Fig.13)

$$C_\rho = \{x_1^\rho, x_2^\rho, \ldots\ldots, x_m^\rho, x_{m+1}^\rho, \ldots\ldots, x_{m+n}^\rho\}, \tag{3.7}$$

$$x_i^\rho \in I'_1,\ i = 1,2,3,\ldots,m, \qquad x_j^\rho \in I'_r,\ j = m+1,m+2,m+3,\ldots,m+n,$$

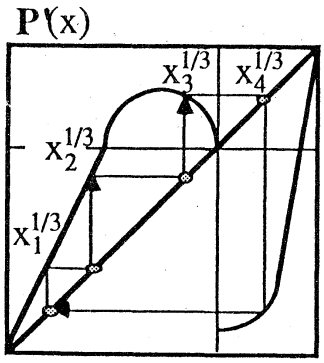

Figure 13

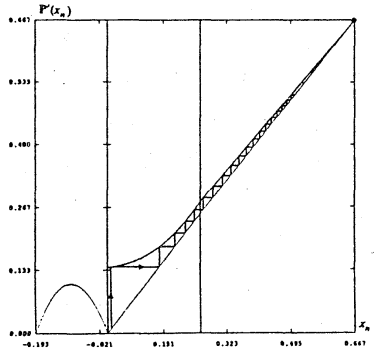

Figure 14 (a)

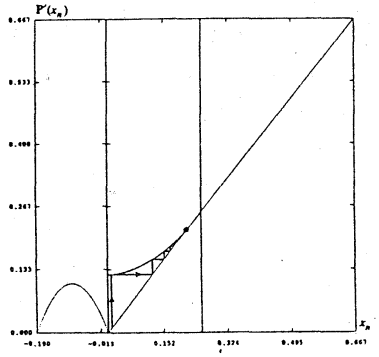

(b)

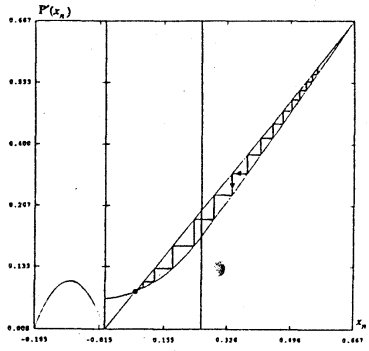

(c)

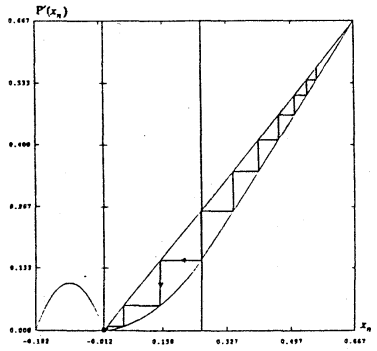

(d)

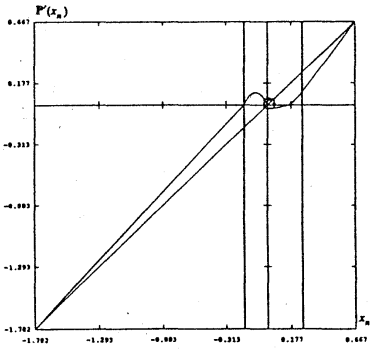

Figure 15 (a)

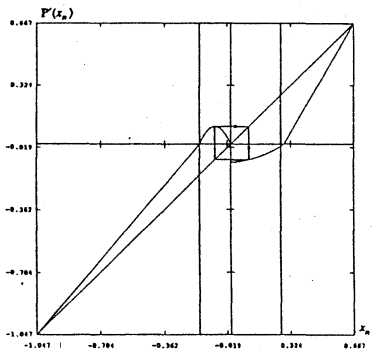

(b)

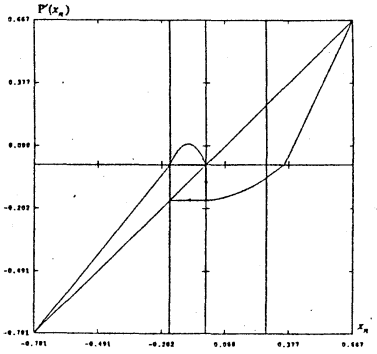

(c)

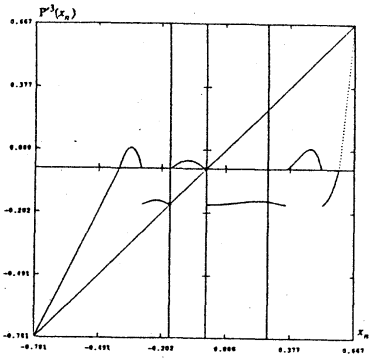

Figure 16 (a)

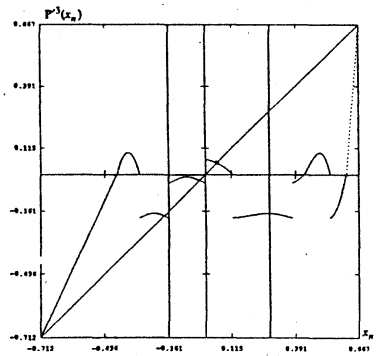

(b)

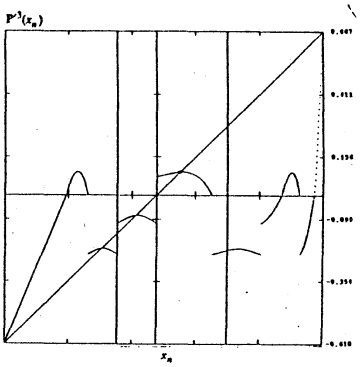

(c)

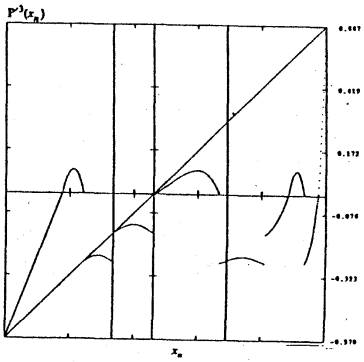

(d)

where interval $\mathbf{I'}_l$ (resp. $\mathbf{I'}_r$) corresponds to fold line (resp.horizontal line). Therefore m (resp. n) sibgnifies the number of jumps (resp. rotation) of the periodic orbit. Note that in (3.7) as well as in Fig.13, the subscript 1,2,...,m,m+1,...m+n do not indicate the iteration steps. We call the orbit defined by (3.7) an *n/m-periodic orbit.* or an *n/m-periodic cycle.*

One can examine stability of this periodic cycle by

$$\lambda_L = \frac{1}{n+m}\sum_{k=1}^{k=n+m} \ln \left| \frac{dP'}{dx} \right|_{x=x_k}$$

If λ_L <0 holds, this periodic cycle is stable, and the range in the parameter space where $\lambda < 0$ is called the "ρ-stability interval". If this cycle passes through an extremum of this map, then $\lambda_L = -\infty$ and such a periodic cycle is called a"super stable periodic cycle". Perez, et al [6] studied the circle map in terms of the stability intervals. We will analyze one-paramter bifurcation of **P'** from a similar point of view.

(a) Hopf bifurcation and 1/0-stability interval

Figure 14(a) shows an enlargement of the x-**P'**(x) graph at c=4.1. The fixed point (x_p, x_p) is clearly stable.

The condition for Hopf bifurcation is given by

$$\left| \frac{dP'}{dx} \right|_{x=x_p} = A_2^2 = 1$$

Note that (3.9) is equivalent to a similar condition in section 2.2. At c=4.0, (3.9) holds, and Figure 14(b) shows the graph in this situation. Note that a fixed point which is stable in the left-hand side region, but which is neutral in the right-hand side region, i.e., semi-stable fixed point, appears in this case, because of piecewise-linearity. As c decreases, this changes into a stable fixed point which corresponds to the 1/0-periodic orbit, namely, $\mathbf{C}_{1/0}=\{x_1^{1/0}\}$. As c decreases, further, $x_1^{1/0}$ gets closer to the origin, (see Fig.14(c)). Note that the stability of this periodic cycle eventually gets stronger in view of the following properties:

(1) $\mathbf{P'}_l(\mathbf{P'}_r(x))$ is monotone increasing,

(2) $\left[\frac{\partial \mathbf{P}_l'(\mathbf{P}_r'(x))}{\partial x} \right]_{x=0} = 0$ holds.

Finally $x_1^{1/0}$ hits the origin at c≅3.646, and $x_1^{1/0} = \mathbf{P'}_l(\mathbf{P'}_r(x)) = 0$. In the constrained system, this means that the unstable manifold $W^u(p_0)$ hits the cusp-point. In other words, a pair of 1/0-periodic orbits hit the cusp-point and merge with each other to form a saddle-connection. Note that the origin is a semi-stable fixed point which is not only stable in the right-hand side region, but also unstable in the left-hand side region (see Fig.14(d)).

(b) 1/1 and 1/2-stability interval

Here, the saddle-connection is broken and transformed into a 1/1-periodic cycle; $\mathbf{C}_{1/1}=\{x_1^{1/1}, x_2^{1/1}\}$.

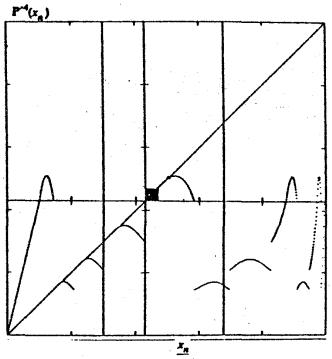

Figure 17 (a)

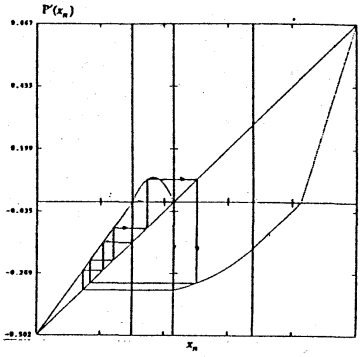

(a)

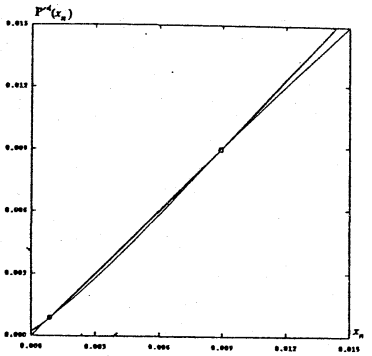

(b)

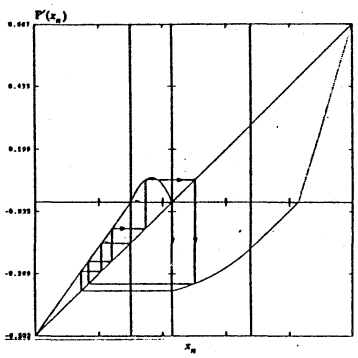

(c)

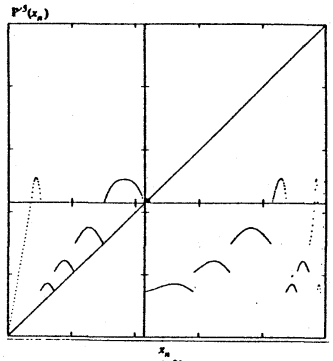

(d)

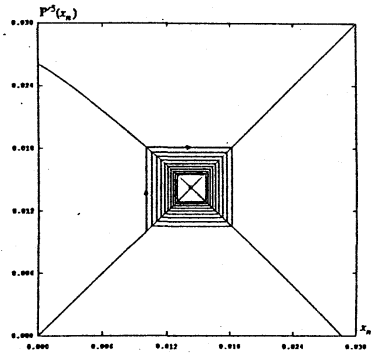

(e)

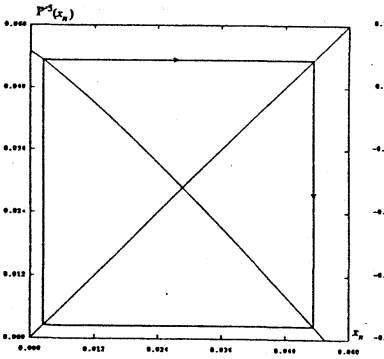

(f)

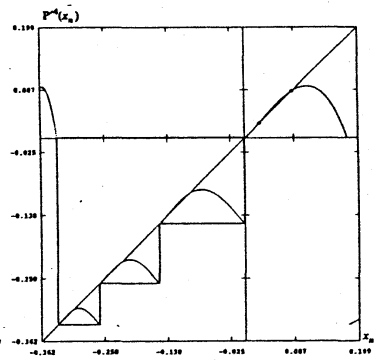

(g)

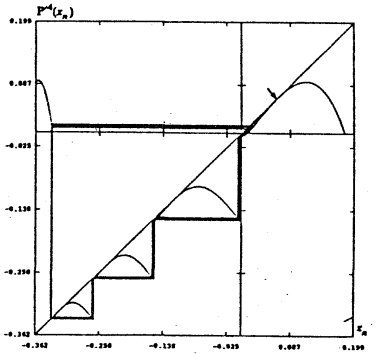

Figure 18 (a)

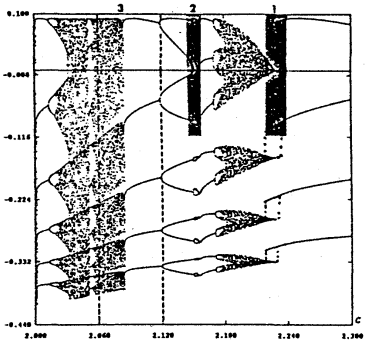

(b)

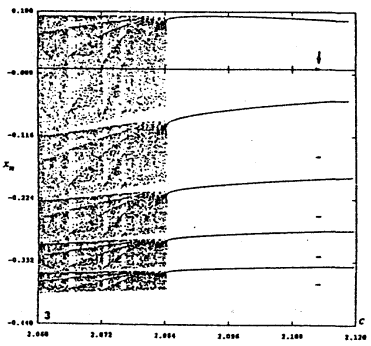

Figure 19 (a)

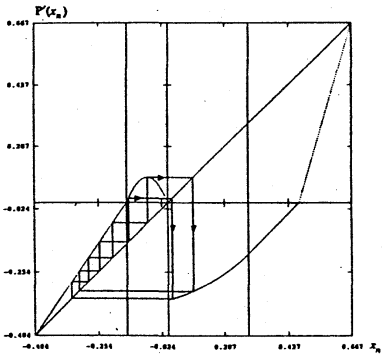

In particular, when $P'_l(P'_r(0))$ becomes negative, the fixed point $x_1^{1/0} = 0$ bifurcates into a pair of periodic points, i.e., $x_1^{1/1}$ and $x_2^{1/1}$, (see Fig.15(a)). Note that they are stable because the 1/1-periodic cycle exists in a neighberhood of the origin. In the constrained system, this process corresponds to the appearance of a periodic orbit which is symmetric with respect to the z-axis via a reverse symmetry-breaking bifurcation. Finally at c ≅3.15, a 1/1-periodic cycle passes through the extremum, and it becomes super stable,(see Fig.15(b)). Then $x_2^{1/1}$ goes back to the origin, and finally it hits the origin in the same manner as the 1/0-periodic cycle at c ≅2.86 does(see Fig.15(c)).

Now we study 1/2-stability interval from another point of view. Figure 16(a) shows the x-$P'(x)^3$ graph corresponding to Fig.15(c), where $P'(x)^3$ denotes the third iteration of $P'(x)$. Note that each periodic point corresponds to a fixed point located at each intersection between the unit slope line and each arch. When a 1/2-periodic cycle, $C_{1/2}=\{x_1^{1/2},x_2^{1/2},x_3^{1/2}\}$, appears, a part of the new arch appears in the righthand-side region from the vertical axis, then a new fixed point, i.e., $x_3^{1/2}$,also appears. As c decreases, this arch gets bigger, and the fixed point asends towards this arch (see Fig.16(c)). Then the fixed point descends from the arch and finally at c ≅2.44 the lefthand-side tip of the arch touches the origin, and hence the origin is a fixed point, (see Fig.16(d)). This situation corresponds to the appearence of a saddle-connection. Then the saddle-connection breaks into a 1/3-periodic cycle, namely, $C_{1/3}=\{x_1^{1/3},x_2^{1/3},x_3^{1/3},x_4^{1/3}\}$.

(c) 1/3-stability interval and bi-stability

Note that the 1/1-stability interval and the 1/2-stability interval , only one fixed point exists in each arch. In the 1/3-stability interval, however, the each becomes tangent to the unit-slope line and three fixed points co-exist for a while. Figure 17(a) shows the co-existence of a pair of 1/3-periodic cycles, i.e., bi-stability. In Fig.17(a), a new periodic cycle, namely, $C'_{1/3}$, appears closer to the origin. But it is difficult to observe an unstable 1/3-periodic cycle, $\underline{C}_{1/3}$. Figure 17(b) shows an enlargement of the square in Fig.17(a). Observe that there are two fixed points: stable fixed point $x'^{1/3}_4 \in C'_{1/3}$ and unstable fixed point $\underline{x}_4^{1/3} \in \underline{C}_{1/3}$. These fixed points are born via a tangent bifurcation. Hence this bifurcation implies the bigining of bi-stability. These two stable periodic cycles bifurcate in different ways. As c decreases, the unstable fixed point $\underline{x}_4^{1/3}$ and the stable fixed point $x_4^{1/3}$ get closer each other, while the new stable fixed point $x'^{1/3}_4$ gets closer to the origin. At c ≅2.2286, $x'^{1/3}_4$ hits the origin and bifurcates into a 1/4-periodic cycle, $C_{1/4}$, in the same manner as in the 1/1 and 1/2- periodic cycle does (see Fig.17(c) and (d)). Then $C_{1/4}$ bifurcates into a 2/8-periodic cycle, via period doubling (see Fig.17(e)). Beyond this, period doubling no longer occurs. Instead, the 2/8-periodic cycle bifurcates into 2/7-periodic cycle after colliding with the origin. Then this periodic cycle bifurcates into another high-period cycle with repeated period doubling and collision with the origin. Finally a band-like chaos appears in a complex manner. Figure 21(f) shows the bi-stability between the band-like chaos and the 1/3-periodic cycle at c ≅2.228. On the other hand, $x_4^{1/3}$ and $\underline{x}_4^{1/3}$ hit and annihilate each other by tangent bifurcation at c ≅2.224. Hence the trajectory starting from the neighborhood where this tangent bifurcation takes place converges into another attractor (see Fig.17(g)). This situation corresponds to the end of bi-stability. Figure 18(a) shows an enlargement of the bifurcation diagram in Fig.12.

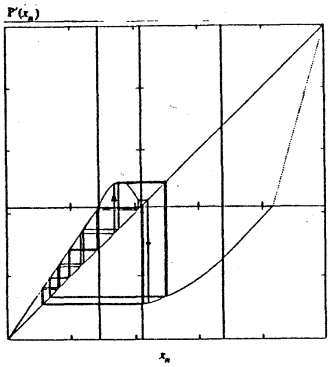

(b)

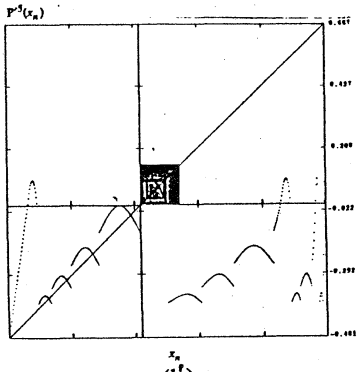

(b)

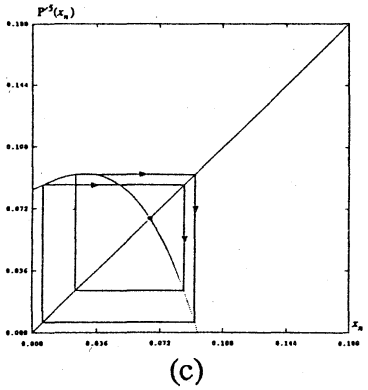

(c)

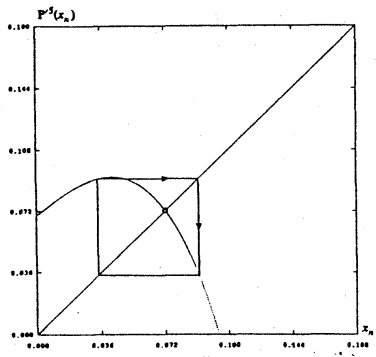

(d)

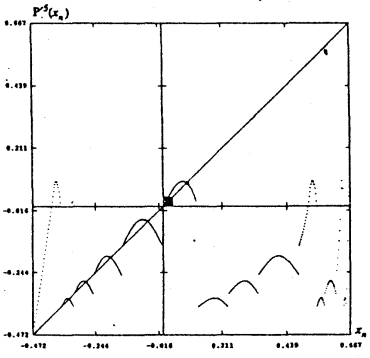

(e)

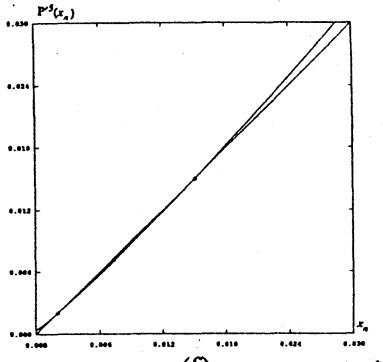

(f)

Figure 20 (a)

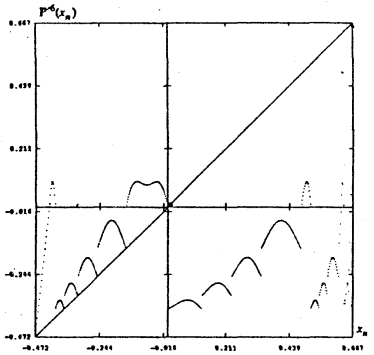

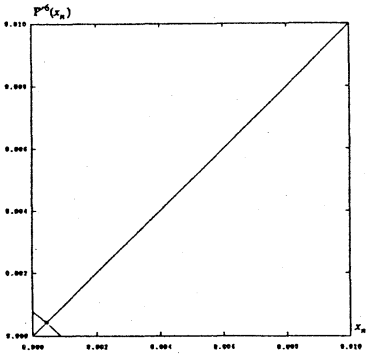

(b)

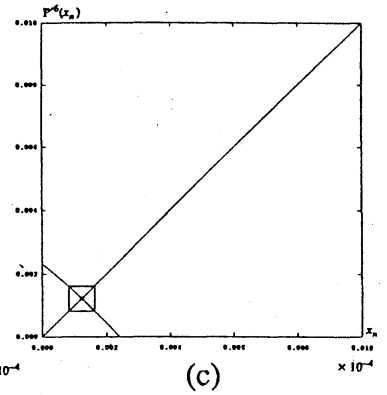

(c)

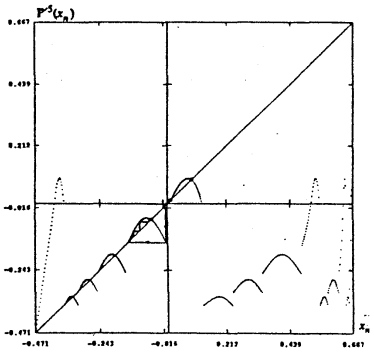

(d)

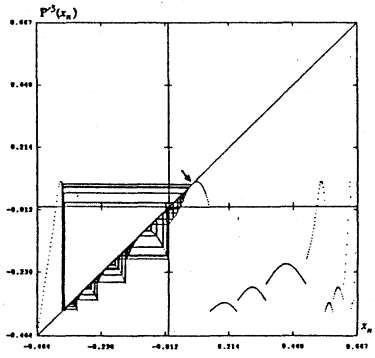

(e)

(d) 1/4-periodic cycle and intermittency

After the disappearence of the 1/3-periodic cycle, many small periodic windows appear and then disappear. Finally, a 2/7-periodic cycle appears via reverse doubling at c ≅2.16, (see Fig.19(a) and 19(b)). Then this periodic cycle bifurcates into a 2/8-periodic cycle upon colliding with the origin, and then it jumps into a 4/15-periodic cycle. Finally, the 4/15-periodic cycle bifurcates into a 4/16-periodic cycle via a collision with the origin. Then reverse period doubling takes place twice, whereupon the 1/4-periodic cycle appears again. Figure 19(c)~(e) shows the reverse period doubling sequence of 4/16-periodic cycle. Note that the 4/16-periodic cycle is confined within an arch of $P'^5(x)$ and the reverse period doubling cascade takes place in the same manner as the logistic map $x_{n+1}= -ax_n(x_n-1)$.

After the second appearence of the 1/4-periodic cycle, we observed the first tangent bifurcation Hence a new stable 1/4-periodic cycle and unstable 1/4-periodic cycle, say $C'_{1/4}$ and $\underline{C}_{1/4}$, are born simultaneously at c ≅2.1129818. Figure 19(f) shows an enlargement of the shaded square of Fig.19(e), where bi-stability is clearly observed. Note that in this case, tangency occurs in a very small neighborhood of the origin. Next we found that $C'_{1/4}$ bifurcates into a 1/5-periodic cycle at c ≅2.11298168, and that the 1/5-periodic cycle bifurcates into a chaotic state in the same manner as $C'_{1/3}$ does, (see Fig.20(a)~(c)). But as soon as the band-like chaos appears, it collides with $\underline{C}_{1/4}$. This implies an interior crisis which leads to the disappearence of the chaotic state, (see Fig.20(d)). In the case of 1/3-periodic cycle, the second tangent bifurcation leads to the end end of bi-stability. Here, however, interior cricis causes the end of bi-stability. If the initial condition is held fixed in the neighborhood of the origin, one can observe an island which corresponds to the band-like chaos in the bifurcation diagram. Figure **18**(b) shows this bi-stability, and its arrow indicates the chaotic island which is corresponding to the band-like chaos. This is the reason we can not find bi-stability in the end of the 1/4-cycle. Then $C_{1/4}$ disappears via the second tangent bifurcation, and chaotic state appears via intermittency, (see Fig.20(e)). The arrow in Fig.20(e) indicates one of the channels.

V. 2-Parameter Bifurcation Analysis

The above observations reveal a striking similality in the structure of the stability intervals. The chaotic region seems to appear inside each interval, and becomes large in the righthand-side region of the each interval as c decreases. In this case chaos does not appear simply via a period doubling sequence. The bifurcation sequence is much more complex. It is very difficult to study this sequence from the one-parameter bifurcation point of view. Hence we imbeded this one-parameter sequence into the (c,α)-parameter space. Let us analyse the structure of each stability interval in this parameter space.

Consider the following important boundaries:

(a) Hopf bifurcation line : $\alpha = 4.0$, (b) Bounday crisis curve : $\alpha = B(c)$,

(c) Critical line : $\alpha = (2c + 4)/3$.

We call the region below the critical line and the region above the critical line the "sub-critical region' and "super-critical region", respectively. Note that in the super critical region, there is no bi-stability because the first tangent bifurcation no longer occurs there, and only an unstable periodic cycle is born.

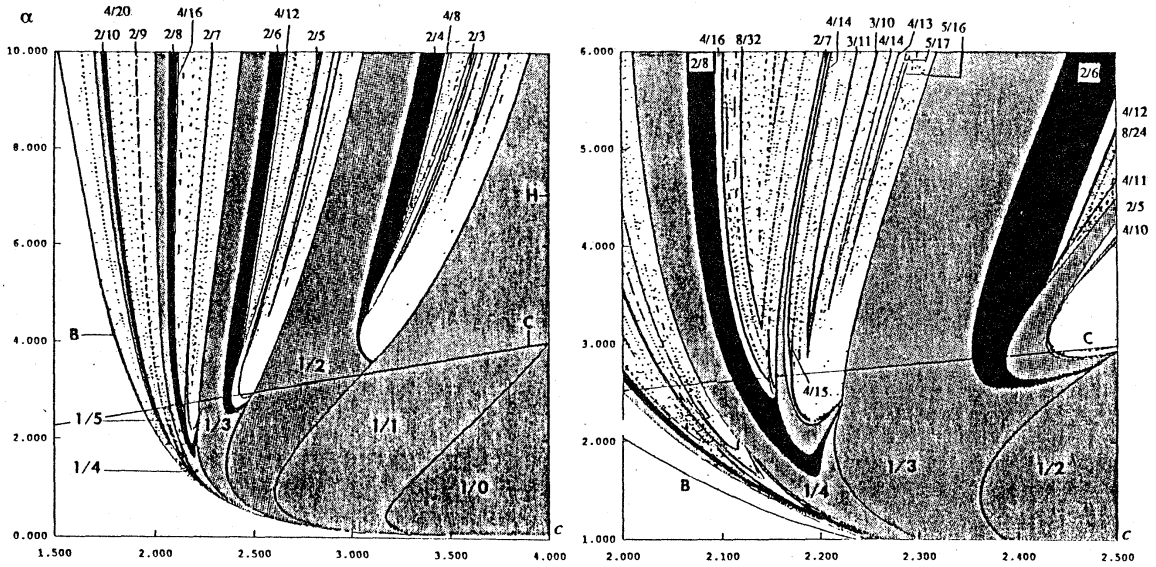
α
4/20
2/10
2/9
4/16
2/8
2/7
4/12
2/6
2/5
4/8
2/4
2/3
10.000
8.000
6.000
4.000
2.000
0.000
1.500
2.000
2.500
3.000
3.500
4.000
B
H
C
1/2
1/5
1/3
1/1
1/4
1/0
c
(a)
4/16
8/32
4/14
3/10
4/13
5/16
2/7
3/11
4/14
5/17
2/8
2/6
4/12
8/24
4/11
2/5
4/10
6.000
5.000
4.000
3.000
2.000
1.000
2.000
2.100
2.200
2.300
2.400
2.500
4/15
1/3
1/2
1/4
B
C
c
(b)

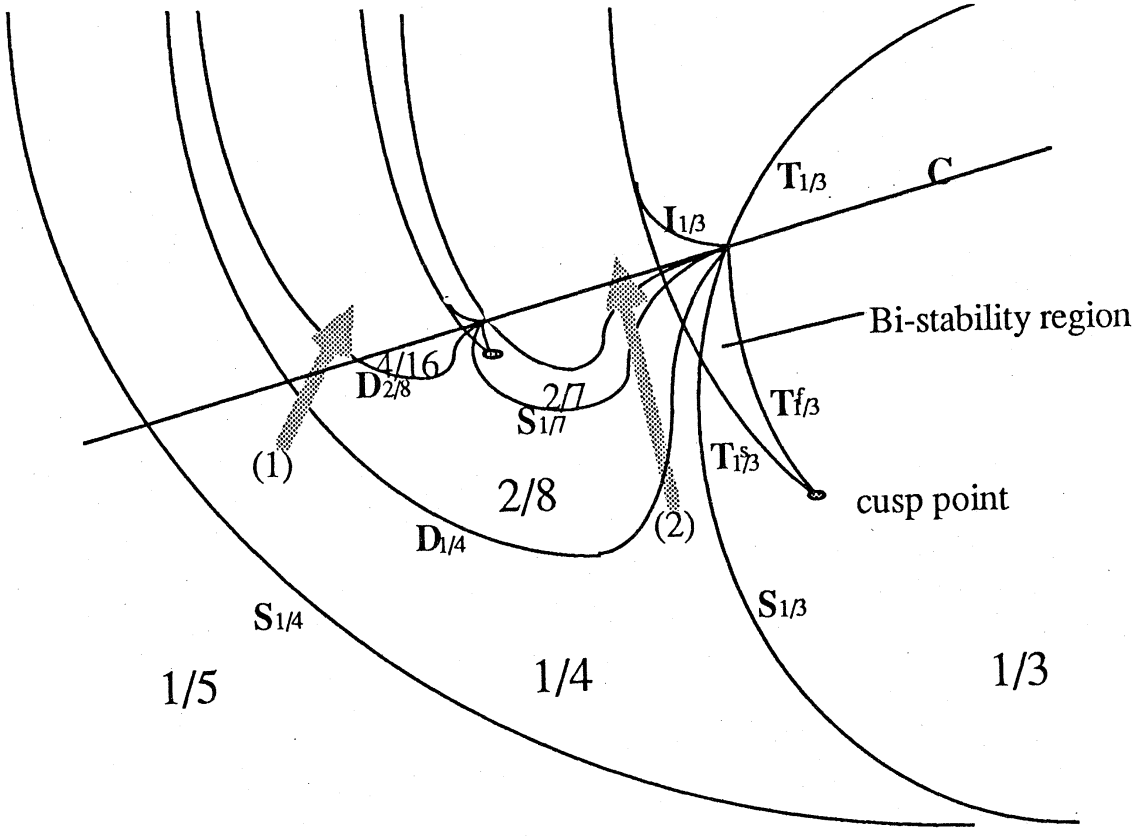
T1/3
C
I1/3
Bi-stability region
4/16
D2/8
2/7
S1/7
Tf/3
T1/3
(1)
2/8
cusp point
(2)
D1/4
S1/3
S1/4
1/5
1/4
1/3

Figure 21 (c)

Figure 21(a) shows the two-parameter bifurcation diagram, where the dotted area corresponds to 1/m-stability interval, the black area corresponds to the region where 2/2m-periodic cycle exists. Each fraction denotes ρ, **H** denotes the Hopf bifurcation line, **B** denotes the boundary crisis curve, and **C** denotes the critical line. Note that the structure of the stability interval is similar to the well-known "Arnold tongue". The boundary $\mathbf{S}_{1/m}$ between the 1/m and 1/m+1 -stability interval implies a symmetry breaking bifurcation or revese symmetry breaking bifurcation. The boundary $\mathbf{D}_{1/m}$ between 1/m and 2/2m - stability interval implies a period doubling bifurcation. The $\alpha = 2.5$ -line corresponds to the one-parameter bifurcation sequence described in the previous section. Note that this line is almost tangent to the $\mathbf{D}_{1/3}$-boundary. This situation corresponds to the tangency between the exponential curve and the horizontal axis which is indicated by an arrow in Fig.20. This is the reason there is no chaotic region between 1/0 and 1/3-stability interval. Figure 21(b) shows the enlargement of a part of Fig.21(a). Now we describe the detail of the 1/4-stability interval.

(1) Interior of the 1/4-stability interval

If one varies the parameter along direction of the arrow (1), the 1/4-periodic cycle bifurcates into a $2^k/4\cdot2^k$-periodic cycle via following period doubling cascade:

$$1/4 \to 2/8 \to 4/16 \to 8/32 \to 16/64 \to 32/128 \to 64/256 \to 128/512 \to \cdots \text{Chaos.} \qquad \text{(S.1)}$$

before chaos appears. On the other hand, if one varies the parameter along direction of the arrow (2) the 1/4-periodic cycle bifurcates first into a 2/8-periodic cycle via period doubling, and then it bifurcates into a 2/7-periodic cycle via a symmtry breaking bifurcation. After this situation, a period doubling and a symmetry breaking take place alternatively. Hence the follwing sequence can be observed:

$$1/4 \to 2/8 \to 2/7 \to 4/14 \to 4/15 \to 8/30 \to 8/29 \to 16/58 \to 16/59 \to \cdots \text{Chaos.} \qquad \text{(S.2)}$$

This sequence corresponds to the process where $\mathbf{C}_{1/4}$ breaks into chaotic state. In the same manner, there are two fates for every $2^k/4\cdot2^k$-periodic cycle. One is to bifurcate into $2^{k+1}/4\cdot2^{k+1}$- periodic cycle via a period doubling, the other is to bifurcate into $2^k/(4\cdot2^k+1)$-periodic cycle or $2^k/(4\cdot2^k-1)$-periodic cycle via symmetry breaking bifurcation. Hence the following sequence can be observed:

$$1/3 \to 2/7 \to 4/15 \to 8/31 \to 16/63 \to 32/127 \to 64/255 \to 128/511 \to \cdots \text{Chaos.} \qquad \text{(S.3)}$$

The relationship between these three sequences can be sumarized by the following schema.

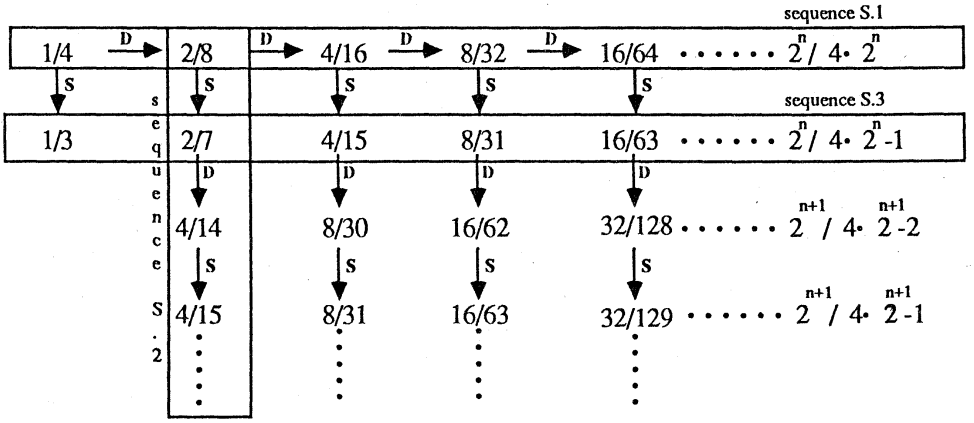

Note that the similar structure which corresponds to the sequence (S.3) seems to obey a Feigenbaum's δ.

(2) Boundaries of the 1/4-stability interval

Recall that the bi-stability takes place on each side of the stability interval. This means theat $S_{1/}$ goes under the 1/3-stability interval, and that this stability interval overlaps with the 1/3-stability interval. In the one-parameter bifurcation, first tangent bifurcation implies the begining of the bi-stability, and the second tangent bifurcation implies the end of the bi-stability. In the two-parameter bifurcation these bifurcation occurs on the curves $T^f_{1/3}$ and $T^s_{1/3}$,respectively. Note that cusp exists between those curves and that each curve starts from a cusp-point. Once hits C, this curve changes its meaning. The curve, $T_{1/3}$ means the birth of 1/3-unstable periodic cycle. There is another important curve , $I_{1/3}$ where interior crisis occurs. $T^f_{1/3}$ and $I_{1/3}$ seem to be tangent to each other on the critical line C, forming $T_{1/3}$, (see Fig.21(c)). The same cusp structure seems to exists between every $2^k/(4\cdot2^k-1)$ and $2^k/4\cdot2^k$ -stability interval.

(3) Period-adding sequence in the chaotic region

In the chaotic region, there are many island-like stability intervals, where the islands all exhibit the same structure. Consider a subset in the parameter space, for example, the a=5.0-line. Observe how the ρ of these islands changes as c increases. For example, the following period-adding sequence can be easily identified:

$$1/4 \rightarrow 2/7 \rightarrow 3/10 \rightarrow 4/13 \rightarrow \cdots\cdots \rightarrow n/3n+1 \rightarrow \cdots\cdots \rightarrow 1/3 . \qquad \text{(S.4)}$$

We conjecture that there exists some kind of relationship between the circle map and the above map. In our future research, the detailes of the stability intervals will be studied.

ACKNOWLEDGMENT

The auther would like to thank Prof.Matsumoto of Waseda University, Prof.Komuro of Numazu College of Technology, Prof. S.Ushiki, Dr.H.Oka of Kyoto University, Prof.A.Sakamoto of Tokushima University for useful discussions.

REFARENCES

[1] H.Oka and H.Kokubu, "Constrained Lorenz-like Attractors", Japan Journal of Applied Mathematics, Vol.2, No.2, pp.495-500, December 1985.

[2] S.Ushiki and R.Lozi,"Organized Confinors and anti-Confinors and their Bifurcations in Constrained "Lorenz" System, University de Nice, Preprint n' 140, Mars 1987.

[3] R.Tokunaga, M.Komuro,T.Matsumoto and L.O.Chua," "Lorenz" Attractor from an Electrical Circuit with Uncoupled Piecewise-Linear Resistors", preprint.

[4] E.N.Lorenz, "Deterministic Nonperiodic Flow", Journal of the Atomospheric Science, 20, PP.130-141, 1963.

[5] K.Kaneko, "On the Period-Adding Phenomena at the Frequency Locking in a One-Dimensional Mapping", Prog.Theor.Phys, Vol.68, No.2, August 1982, Progress Letters.

[6] L.Glass and R.Perez,"Fine Structure Phase Locking", Phys. Rev. Lett., Vol.48, No.26, pp.1772-1775, June 28, 1982